16th World Conference on Earthquake Engineering, 16WCEE 2017
Santiago Chile, January 9th to 13th 2017
Paper N° 1503 (Abstract ID)
Registration Code: S-Y1464444858

Verification of seismic response reduction by real-time hybrid simulation of a mid-story isolation with a magnetorheological rotary inertia mass damper

H. Fujitani[(1)], Y. Mukai[(2)], S. Yoshida[(3)], M. Ito[(4)] , Y. Sato[(5)]

[(1)] *Professor, Kobe University, fujitani@kobe-u.ac.jp*
[(2)] *Associate Professor, Kobe University, ymukai@port.kobe-u.ac.jp*
[(3)] *Former graduate student, Kobe University, syouheeeeeei@yahoo.co.jp*
[(4)] *Assistant Professor, Kobe University, mai.ito@goldt.kobe-u.ac.jp*
[(4)] *Mechanical engineer, Sanwa Tekki Corporation, sato-t@tekki.co.jp*

Abstract

Base-isolation systems show high performance of reduced floor acceleration and deformation of superstructures during periods of strong earthquake ground motion. However, against near-fault pulse ground motions of intra-plate earthquakes or long-period ground motions of inter-plate earthquakes, results of recent studies show that excessive displacement occurs in the base-isolation layer.

A mid-story isolated system presents the benefit that the isolation layer is constructed mid-story: structural systems often differ between lower stories and higher stories. As described herein, the seismic response reduction performance of mid-story isolated buildings attributable to a semi-active control system was investigated using real-time hybrid simulation by a shaking table. A six-lumped-mass model simplifies the multi-story building with an isolation layer mid-story.

Real-time hybrid simulation using an actual damper (2 kN max. damping force) and a four-story structural model (2 ton total weight) of the superstructure was conducted to verify the seismic response reduction performance of the system. The two-story structural model response under the isolation layer of the system was calculated using a digital signal processor (DSP), accounting for both the ground motion and the actual damper force in real time. In this real-time hybrid simulation, the calculation accuracy and time lag are also discussed.

A semi-active control method using a rotary inertia mass damper filled with magnetorheological fluid (MR fluid) was proposed. The damper shows both a mass amplification effect attributable to rotational inertia and a variable damping effect attributable to the MR fluid. The damping force is controlled by the strength of the magnetic field applied to the MR fluid. The magnetic field strength is determined by the electric current, which is calculated using the proposed semi-active control method based on the respective velocities of the ground motion and of the isolation layer relative to the layer immediately underneath it.

Real-time hybrid simulation results suggest that the response displacement of the structure above the isolation layer is reduced considerably without increasing the response acceleration of the entire structure against near-fault pulse and long-period ground motions. The proposed semi-active control using an MR rotary inertia mass damper was confirmed to be effective for mid-story isolated buildings. The control method achieves the objectives.

Keywords: real-time hybrid simulation; semi-active control; isolated structure; near-fault and long-period ground motions

1. Introduction

The large ground motion of the Hyogo-ken Nambu Earthquake of 1995 damaged numerous structures and killed or injured many people. Since this earthquake, the dissemination of isolated structures has advanced rapidly. However, it is thought that isolated structures will respond resonantly with the long period ground motion that would be produced by the Nankai Trough Earthquake or other inter-plate earthquakes that have been predicted in recent years. This would cause excessive deformation of the isolation layer or increase the floor response acceleration. The near fault ground motion caused by an intra-plate earthquake will force excessive displacement

of the isolation layer [1]. Semi-active control, which can vary the vibration characteristics, is considered to be one measure of resolving this problem.

When verifying the effectiveness of semi-active control by analysis, the uncertainty accompanying the modeling of the control force variable damper is a problem. Thus, authors have performed numerical analysis of structural parts that can be easily and precisely modeled to propose a real-time hybrid simulation [2-9] that can perform real-time shaking of a semi-active control device that includes many uncertain elements and is velocity-dependent. This paper proposes a real-time hybrid simulation using a shaking table. This method permits the use of structural parts other than dampers as the test specimens. For example, authors work on a mid-story isolated building as the structure model.

On the other hand, in recent years, research has been undertaken on methods of reducing the response displacement due to the inertial mass effect that causes inertia proportional to the relative acceleration in order to control deformation of the isolation layer. This study uses a damper that encapsulates magneto-rheological fluid (MR fluid) as the rotary inertia mass damper that is relied on to have an inertia mass effect (hereinafter referred to as “MR rotary inertia mass damper”) as the semi-active control device. Previous research using this control device [5, 6, 9] has not resolved the challenge of evaluating the control time lag.

Based on such background conditions, this study tested semi-active control using the MR rotary inertia mass damper, which is a semi-active control device with a unique mechanism and properties. A real-time hybrid simulation system was built to be the hypothetical building by combining a shaking specimen of a mid-story isolated building and a multi-mass model using a computer. The validity of the system was then verified.

2. Real time hybrid simulation

Figure 1 is a photo of the shaking table and test specimen. Table 1 shows the specifications of the shaking table. The object of the simulation is a mid-story isolated building. Figure 2 is a schematic diagram of the application of the mid-story isolated building to the simulation. The test specimen consists of an isolation layer and superstructure, while the substructure (structure under the isolation layer) is modeled using a computer. Figure 3 is a schematic diagram of the real-time hybrid simulation. The test specimen of the superstructure consists of four floors, as shown in the photo in Figure 1, and the substructure calculated by DSP (AD5436-I7 from A&D Company Limited) in a computer is a two-mass system. The stiffness of the spring of the first layer of the test specimen is small, corresponding to the isolation layer. First, earthquake ground motion is caused to act on the mass system model inside the DSP to perform a time-history response analysis. The absolute displacement of the top mass (the floor under the isolation layer) of the two-mass system obtained in this way is reproduced by commanding the shaking table. The spring reaction and damping force of the damper installed on the isolation layer of the test specimen are input back to the two-mass system on the DSP to be used for the time-history response analysis. The response of the test specimen and the two-mass system on the DSP are both successfully recorded, and their values are used to perform semi-active control.

These operations are repeated at 500 Hz intervals to perform the hybrid simulation. This permits real-time hybrid simulation that considers the entire control force of the damper produced by the force acting between the superstructure and substructure, as well as by semi-active control.

Fig. 1 – Shaking table and test specimen

Table 1 – Specification of shaking table

Maximum force (when mass is 5,000kg)		70 kN	(Sinusoidal)	140 kN	(Random)
Maximum Acceleration (when mass is 5,000kg)		10 m/s^2	(Sinusoidal)	20 m/s^2	(Random)
Maximum Velocity (when mass is 5,000kg)		1.0 m/s	(Sinusoidal)	1.5 m/s	(Random)
Maximum Displacement	±275 mm	Pay load	10,000 kg	Table size	2.0×3.0 m

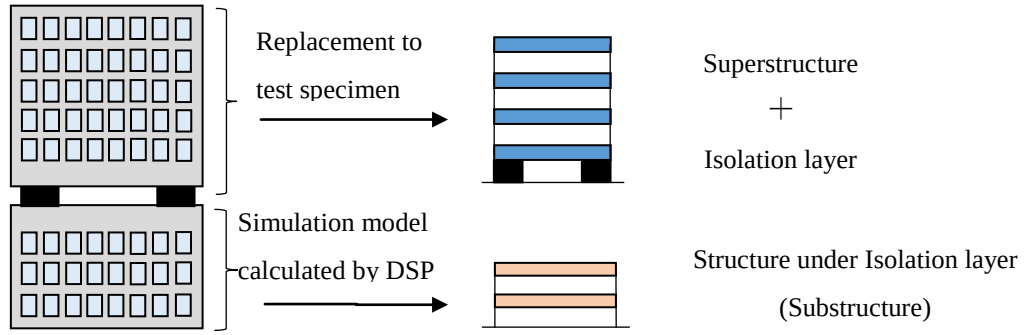

Fig. 2 – Concept of modeling of a mid-story isolation for real-time hybrid simulation

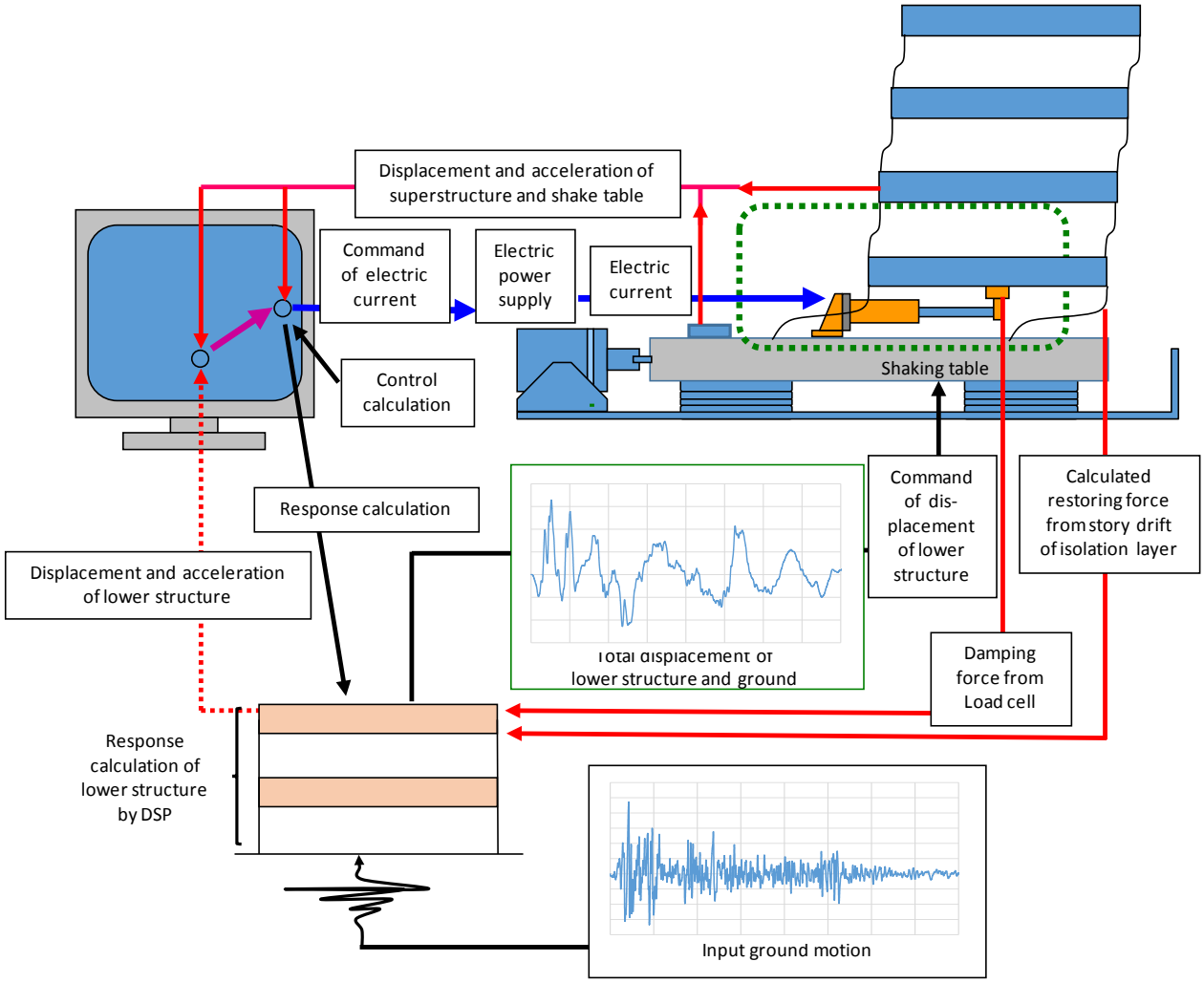

Fig. 3 – Diagram of real-time hybrid simulation by using shake table of a mid-story isolation

3. MR rotary inertia mass damper and the test specimen

3.1 Outline and modeling of the damper

Figure 4 shows the structure of the MR rotary inertia mass damper [1, 9, 10], Figure 5 is a schematic diagram of generating damping force, and Figure 6 is a schematic of the force-displacement relationship. Table 2 shows the design specifications of the damper. In the force generation part of the MR rotary inertia mass damper, linear motion is converted to rotating motion predominantly by ball screws and ball nuts. Rotation of the flywheels on the tip of the ball screws generates a rotary inertia force that is proportional to the relative acceleration in the axial direction. Shear velocity is developed according to the relative displacement between the flywheel and the case. In this way, it is possible to simultaneously obtain the inertia force and the damping force according to the resistance to the shear flow of the MR fluid filling the space around the flywheel. In the case encapsulating the MR fluid, a magnetic field generating mechanism (using an electro-magnet) is attached. By varying the strength of the magnetic field acting on the MR fluid, the resistance to the MR fluid is set freely within a certain range, permitting adjustment of the damping force.

Sinusoidal excitation of a single MR rotary inertia mass damper was conducted in combinations of three excitation frequencies of 0.2, 0.333, and 0.5Hz; two amplitudes of 100 and 200 mm; and six amperages: 0, 0.25, 0.50, 0.75, 1.00, and 1.25 A. The elements of the damper that are modeled consist of the three elements shown in Figure 7 (inertia mass element, viscous damping element, and Coulomb's variable friction element according to the yield shear stress of the MR fluid). Eq. (1) constitutes the modeling.

$$F = m'\ddot{x} + C\dot{x}^{\alpha} + F_{MR} \tag{1}$$

F: damper force, m': equivalent mass of the inertia mass damper, C: viscous damping coefficient of the MR fluid, α: constant ($0 < \alpha < 1$), F_{MR}: force by yield shear stress of MR fluid, and x: displacement of the damper

The modeling is based on force obtained by the damper test. The design value of equivalent mass is 250 kg, but the value m' = 241 kg is obtained. F_{MR} is defined by the secondary formula of the electric current value according the method of least squares. Eq. (2) shows the F_{MR} value that was obtained.

$$F_{MR} = 614I^2 + 316I + 172 \quad \text{(N)} \tag{2}$$

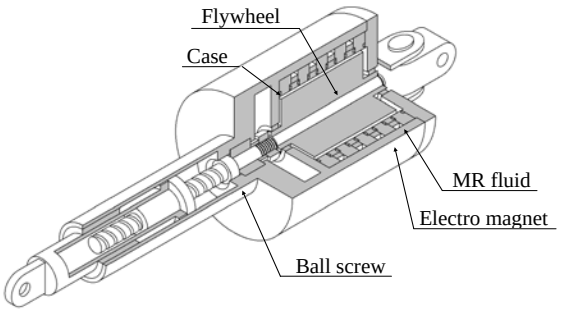

Fig. 4 – Magnetorheological (MR) rotary inertia mass damper

Table 2 – Specification of magnetorheological rotary inertia mass damper

stroke	600（±300）mm
Maximum damping force	2.45×10^3 N
Rotary inertia mass	0.250×10^3 kg
Maximum acceleration	9.80 m/s^2
Maximum velocity	1.00 m/s

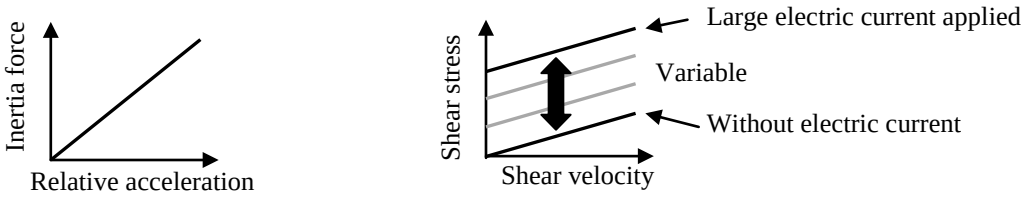

(a) Inertia force – relative acceleration (b) Shear stress of MR fluid – Shear velocity

Fig. 5 – Components of damper force

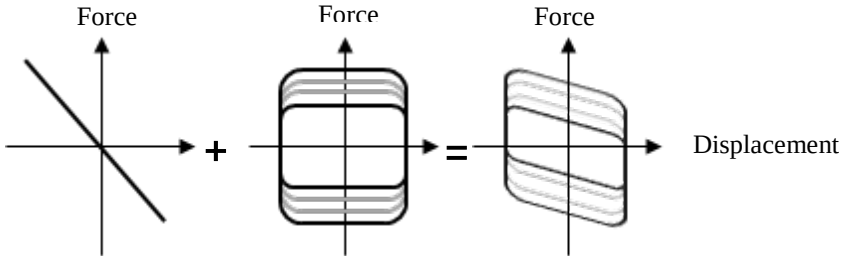

(a) by Inertia mass (b) by viscosity and friction (c) Total damping force

Fig. 6 – Restoring force characteristics of MR rotary inertia mass damper

Then, viscous damping coefficient C and α are obtained. α is fixed and C is obtained by the method of least squares for each α, where the final value of α is that obtained when the standard differential of C is at a minimum. The viscous damping coefficient C is the average of the C values obtained according to determined α values. The values of C and α obtained by this method are 541 Ns/m and 0.679, respectively. The approximation equation of the damping force of the damper is shown as Eq. (3).

$$F = 241\ddot{x} + 541\dot{x}^{0.679} + (614I^2 + 316I + 172)\cdot \mathrm{sign}(\dot{x})\ (\mathrm{N}) \qquad (3)$$

The first, second, and third terms are the inertia mass effect, viscous damping effect, and force according to the yield shear stress of the MR fluid, respectively. Figure 8 compares the test results with those from the approximation equation. The solid line is the test result and the dotted line is the approximation equation result, both of which generally conform. This confirms the validity of the approximation equation.

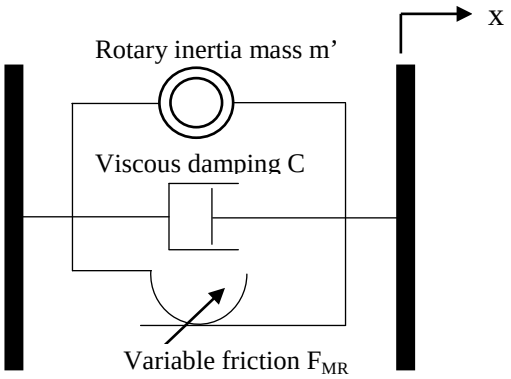

Fig. 7 – Modeling of MR rotary inertia mass damper

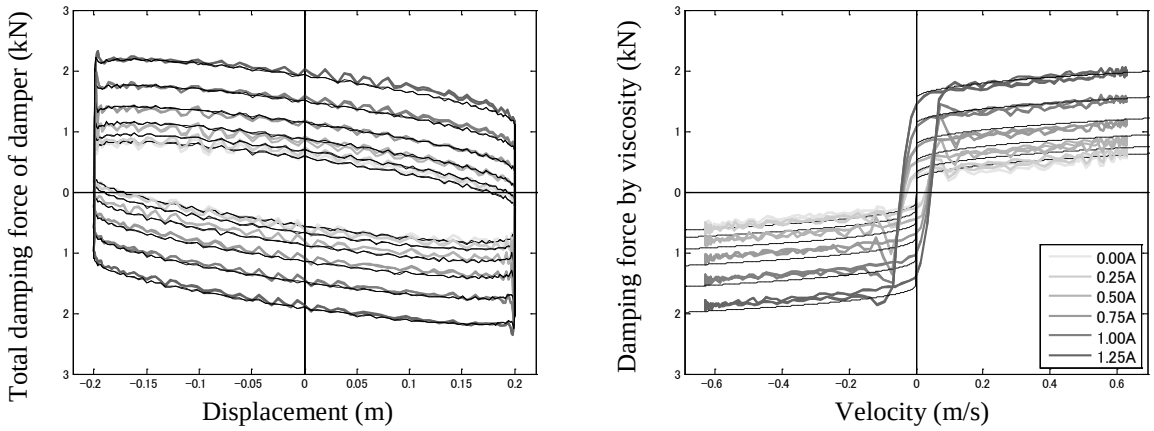

Fig. 8 – Comparison of experimental results and simulated results by Eq. 3

Table 3 – Specification of test specimen

Story	Mass (kg)	Stiffness (N/m)	Viscous damping coefficient (Ns/m)
4	386	95.2×10^3	158
3	475	112×10^3	353
2	471	139×10^3	706
1	695	9.81×10^3	169

4. Semi-active control law

4.1 Proposed control law

Authors propose a control law. This law is applicable when the rotating inertia mass damper is in the phase that increases the absolute velocity of the isolation layer. The increase of the absolute velocity of the isolation layer occurs when the inertia force of the inertia mass has the same sign. It is assumed that because the inertia force acts in the opposite direction to the damper velocity, the absolute value increases when the damper acceleration and absolute velocity have different signs. Thus, at the time of such a phase relationship, in order to eliminate the inertia mass effect, the electric current value that should be used will be reverse calculated based on the modeling formula (Eq. (3)) of the damper and on Eq. (4), according to the relative acceleration.

$$241\ddot{x} + (614I^2 + 316I + 172)\cdot \mathrm{sign}(\dot{x}) = 0 \tag{4}$$

Regarding electric current value I, based on $0 \le I \le 1.25$, $\ddot{x}$ and $\dot{x}$ must have different signs. If this is considered, Eq. (4) becomes Eq. (5).

$$-241|\ddot{x}| + (614I^2 + 316I + 172) = 0 \tag{5}$$

If Eq. (5) is solved for I, Eq. (6) is obtained.

$$I = -0.246 + \frac{\sqrt{1545|\ddot{x}| - 853}}{61} \tag{6}$$

However, $\ddot{x}\cdot\dot{x} < 0$ and $\ddot{x}\cdot(\dot{x}+\dot{z}) < 0$

4.2 Current value decision equation according to ground velocity

The electric current value decision equation proposed here considers the scale of the ground motion, which, here, is the ground velocity. Eq. (7) is used so that the center of the curvature of the velocity–electric current value relational curve changes with a ground velocity of 0.5 m/s as the boundary.

$$I = G_0 \cdot \left|\dot{x}\right|^{(\dot{z}+0.5)} \tag{7}$$

z represents the ground displacement. Figure 9 is a schematic of the electric current value decision equation. During ground motion with a maximum ground velocity of 0.5 m/s, at the stage where a high damping gradient is provided and the response is small, sufficient control force is generated. Conversely, during ground motion with a ground velocity greater than 0.5m/s, the response is large. Thus, the aim is a gentle response on a low damping gradient. If the two control rules in Chapter 4 are combined, Eqs.s (8) to (11) are obtained, where it is assumed that $G_0 = 1$.

$$I = I_1 \quad \text{When } \ddot{x} \cdot \dot{x} < 0 \text{ and } \ddot{x} \cdot (\dot{x} + \dot{z}) < 0 \tag{8}$$

$$I = I_2 \quad \text{In other cases} \tag{9}$$

$$I_1 = G_0 \cdot \left|\dot{x}\right|^{(\dot{z}+0.5)} - 0.246 + \frac{\sqrt{1545\left|\ddot{x}\right| - 853}}{61} \tag{10}$$

$$I_2 = G_0 \cdot \left|\dot{x}\right|^{(z+0.5)} \tag{11}$$

5. Comparison results and reproducibility of the real-time hybrid simulation

5.1 Comparing real-time hybrid simulation and numerical analysis

Based on the semi-active control law presented in Section 4, a real-time hybrid simulation was conducted. Table 4 shows the input ground motions. Each input ground motion is a value determined by the limit of the shaking table and specimen. First, the impact of the control time lag, on the control force of the damper is studied. Figure 10 shows the time-history waveform of the control force in a numerical analysis assumed to not consider the simulation results and lag time. The time axis expands between 0.1 and 0.2 s before and after the control force is at a maximum. In a simulation considering the time lag, the times of the rise at 2.16 s and the fall at approximately 2.19 s conform to the simulation values. Considering control time lag in this way permits more precise analysis. The later analyses all considered control lag times.

(a) when V_{ground} is smaller than 0.5 m/s (b) when V_{ground} is larger than 0.5 m/s

Fig. 9 – Concept of ditermination of electric current value

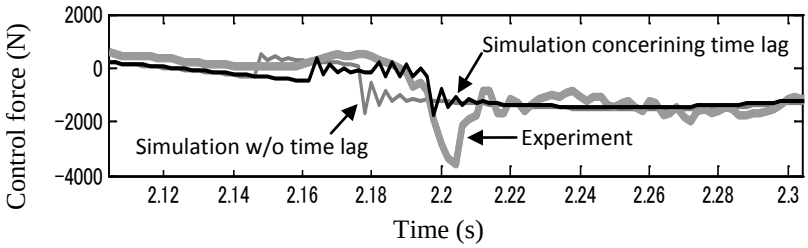

Fig. 10 – Comparison of damping force between real-time hybrid simulation and numerical analysis

Next, the responses of the test specimen and the mass system (substructuire) in the DSP in the real-time hybrid simulation were compared with the responses obtained by numaerical analysis of the entire building. Figure 11 shows the story drift of each story and Figure 12 shows the time-history of the floor accelerations. Table 5 shows the specifications of the two-mass system in the DSP, which corresponds to the substructure of the mid-story isolated building model. The simulation values in Figure 11 and in Figure 12 are, calculated values of the mass system model inside the DSP for the first and second story, respectively. The third to sixth stories represent floor levels 1 to 4 of the test specimen, respectively, and correspond to the response of the superstructure.

The numerical analysis is a result of completely modeling the test specimen, the substructure and the MR rotary inertia mass damper. There are a significant number of places where the entire wave forms are superimposed, confirming that the real-time hybrid simulation and numerical analysis generally are in agreement. This shows that the test specimens and modeling of the dampers are valid, and that the real-time hybrid simulation system was appropriately constructed.

5.2 Reproducibility of the real-time hybrid simulation

The real-time hybrid simulation was a calculation of a mass system of the substructure conducted in real time in the DSP, and commanding the absolute displacement created in the top story of the substructure to reproduce it on a shaking table. The displacement commanded at this time, the reproduced displacement, and the acceleration, are compared. The acceleration waveforms conform closely, revealing that the response generated in the substructure can be followed appropriately. In addition, the shaking table moved according to the displacement instruction, and thus, the reproducibility is also judged to be high.

These are confirmed numerically. The study is conducted based on the correlation coefficient ρ and the RMS ratio ([RMS of reproduced value] / [RMS of ordered (target) value]). The correlation coefficient ρ and RMS are defined by Eqs. (12) and (13), respectively.

$$\rho = \frac{\frac{1}{N-1}\sum_{i=1}^{N}(A_i - \mu_A)(B_i - \mu_B)}{\sqrt{\frac{1}{N-1}\sum_{i=1}^{N}(A_i - \mu_A)^2}\sqrt{\frac{1}{N-1}\sum_{i=1}^{N}(B_i - \mu_B)^2}} \tag{12}$$

$$RMS[A] = \sqrt{\frac{1}{N}\sum_{i=1}^{N}A_i^2} = \sqrt{\frac{A_1^2 + A_2^2 + \cdots + A_N^2}{N}} \tag{13}$$

N: number of data, A_i、B_i: time-history data (corresponding to displacement or acceleration of the reproduced value or command (target) value), μ_A, μ_B: average value of A and B

Table 4 – Input ground motions

Input ground motion		Max. velocity (m/s)	Max. acceleration (m/s^2)
Ground motions used for structural design of buildings	El Centro 1940 NS (90%)	0.30	3.08
	Hachinohe 1968 NS (147%)	0.50	3.33
	BCJ L2 (50%)	0.25	1.82
Near-fault pulse ground motions	JMA Kobe 1995 NS (30%)	0.27	2.46
	JR Takatori 1995 NS (40%)	0.49	2.42
	UMT A4_B2EW (30%)	0.30	1.16
Long-period ground motions	Tomakomai 2003 NS (60%)	0.29	0.84
	Future Nankai (40%)	0.28	1.00

Table 5 – Specification of test specimen

Story	Mass (kg)	Stiffness (N/m)	Natural period (s)	
2	750	250×10^3	First mode	0.53
1	800	300×10^3	Second mode	0.21

Table 6 – Correlation of coefficient and Ratio of RMS of response of shaking table

	Dsplacement of shake table		Accelerarion of shake table	
	Correlation coefficient	Ratio of RMS of measured to command	correlation coefficient	Ratio of RMS of measured to command
El Centro	0.998	0.984	0.966	0.995
Hachionohe	0.998	0.984	0.942	1.011
BCJ L2	0.999	0.985	0.968	1.005
JMA Kobe	0.992	0.978	0,950	0.996
JR Takatori	0.997	0.978	0.973	0.997
UMT A4	0.999	0.986	0.694	1.001
Tomakomai	0.999	0.986	0.917	1.008
Future Nankai	0.999	0.986	0.843	1.043

Table 6 shows the command displacement and actual reproduced displacement of the shaking table, the correlation coefficient of the target acceleration and reproduced acceleration, and the RMS ratio. The correlation coefficient is in a range from –1 to 1, showing that the closer it is to 1, the stronger the positive correlation, and it is suitable for confirming the displacement of the phase. RMS confirms the scale of the absolute value of the time-history response. It is thought that the closer the correlation coefficient and RMS ratio are to 1, the higher the reproducibility. The acceleration was calculated using values at intervals of approximately 3 s, which shows the maximum value. It is confirmed that for every case in which both the correlation coefficient and RMS ratio are close to 1, numerically confirming the displacement is highly reproducible.

These show that the displacement commanded to the shaking table from the DSP is extremely highly reliable. Regarding the acceleration, according to the RMS ratio, highly precise reliability of all the earthquake ground motions is shown. However, there are cases where the correlation coefficient shows a lower value under ground motion: UMTA4 and the Future Nakai Earthquake.

6. Conclusions

In this study, the damper of an isolated layer and the superstructure as specimens of a mid-story isolated building are used to perform a real-time hybrid simulation to calculate the response of the substructure with a mass system model inside the DSP. The validity of this simulation system is verified. The results clarify the following:

(1) The displacement commanded to the shaking table and the reproduced displacement are highly correlated and the RMS values also conform well, indicating high reproducibility

(2) The acceleration is highly correlated with the RMS values, but there are cases where, according to the earthquake motion, the correlation is slightly poor.

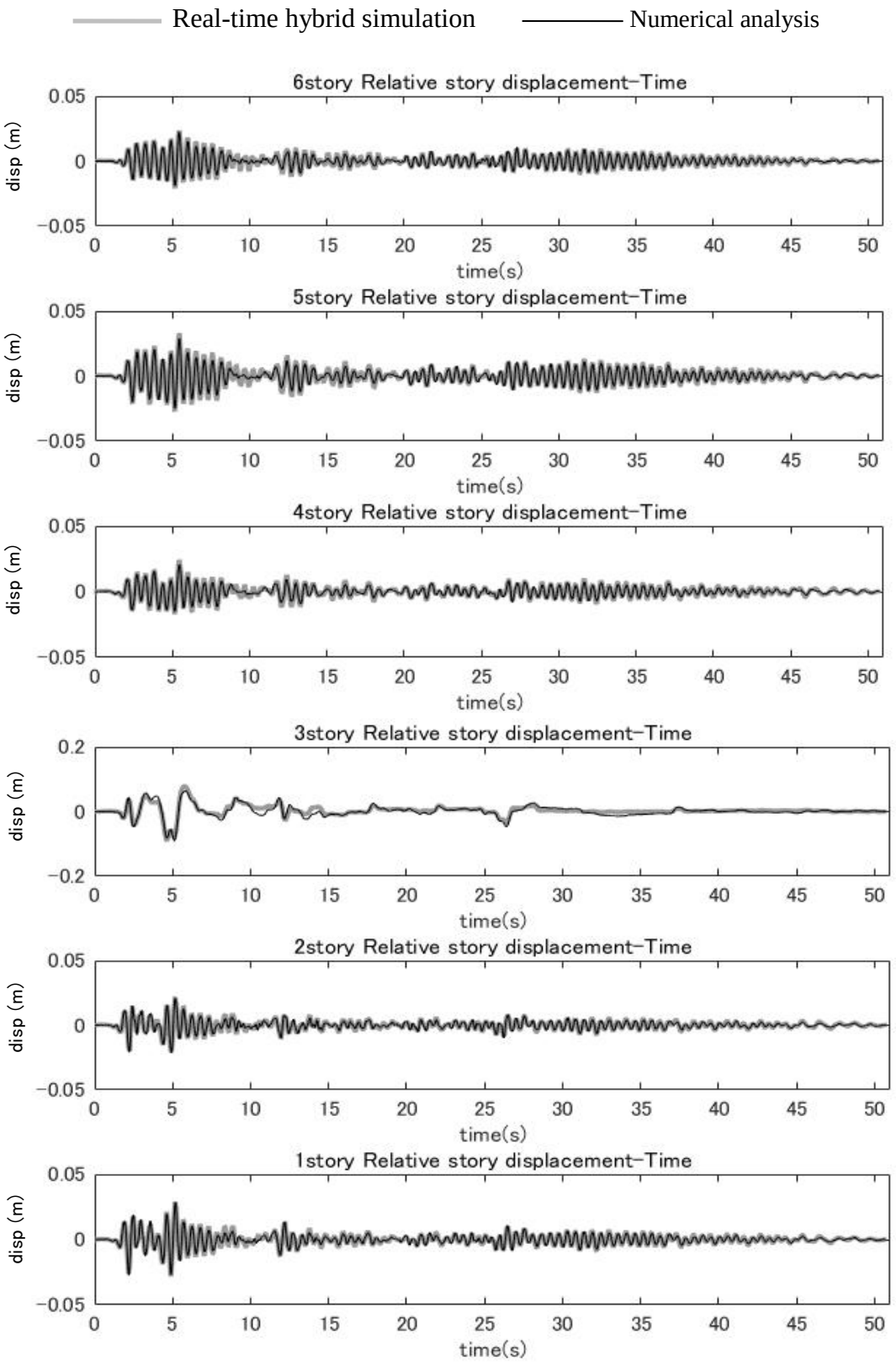

Fig. 11 – Comparison of story drift between real time hybrid simulation and numerical analysis (El Centro 1940 NS)

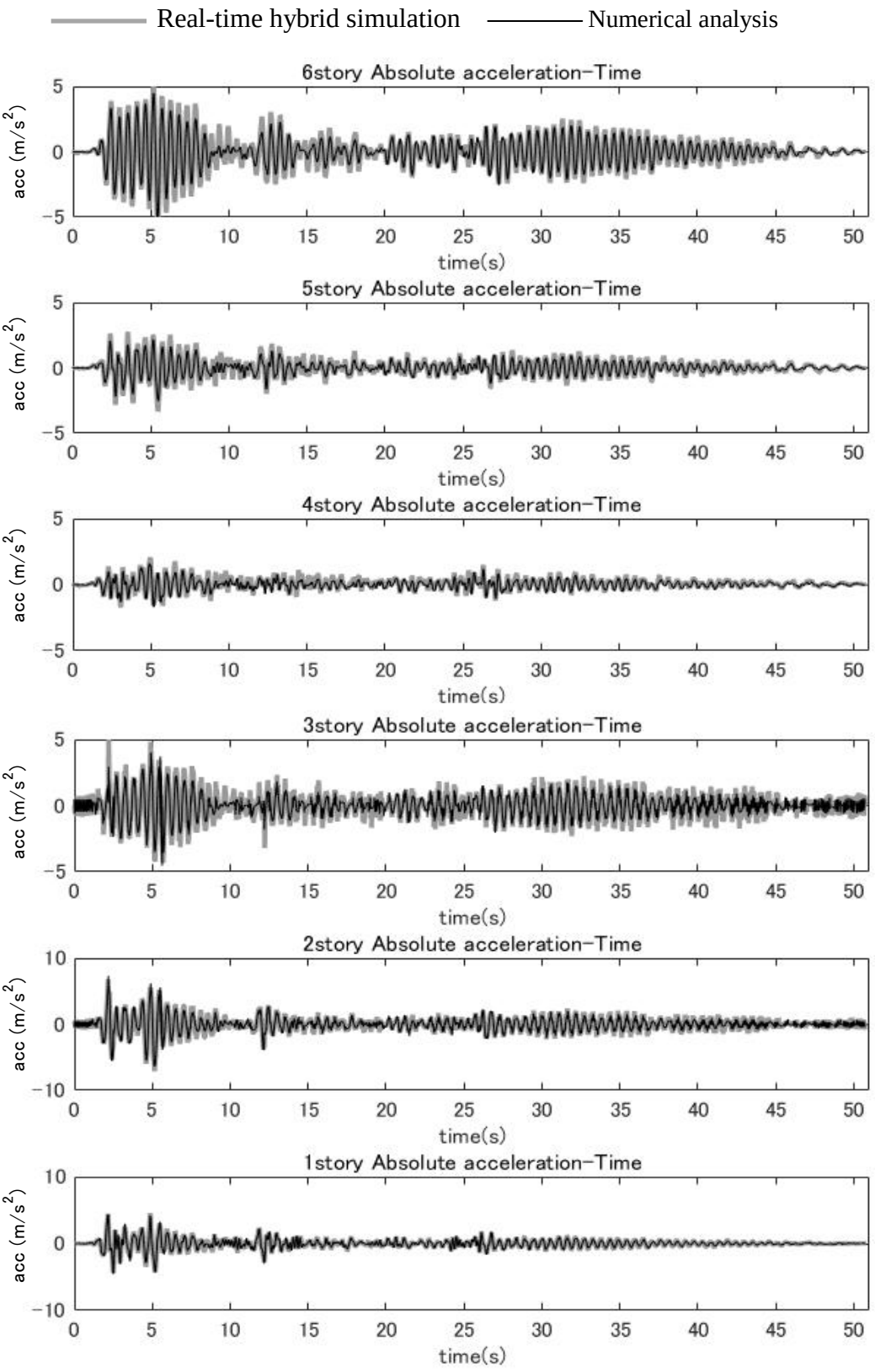

Fig. 12 – Comparison of floor acceleration between real time hybrid simulation and numerical analysis (El Centro 1940 NS)

(3) Semi-active control was performed to study the time lag. It is possible to obtain analysis results similar to those of the real-time hybrid simulation considering the control time lag.

(4) The results obtained by the real-time hybrid simulation that used a mid-story isolated building as the model were compared with the time-history response analysis results for the entire building modeled for all stories, showing good conformity.

The above facts verify the suitability of the modeling of the damper and structure specimen and the real-time hybrid simulation system proposed by this research.

Acknowledgements

Part of this research was supported by the Grant in Aid for Scientific Research (C) of the Japan Society for the Promotion of Science (JSPS KAKENHI Grant Number 23560672)., and the MR rotating inertia mass damper used for the study was manufactured with the assistance of Sanwa Take Corporation. The authors wish to express their gratitude for this support.

References

[1] Fujitani H, Mukai Y, TOMIZAWA T, Hirata K, Mazurka Y, Fuji H (2012): Response reduction of base-isolation system against near-fault pulse and long-period ground motions, Proceedings of 15th World Conference on Earthquake Engineering, No.2002.

[2] Wu B, Wang Q, and Shing B, Our JP (2007): Equivalent force control method for generalized real-time substructure testing with implicit integration, *Earthquake Engineering and Structural Dynamics*, Vol.36, 1127-1149.

[3] Christenson R, Lin Y, Emmons A, Bass, B (2008): Large-scale experimental verification of semiactive control through real-time hybrid simulation", Journal of Structural Engineering, ASCE, Vol.134, No.4, pp.552-534.

[4] Ahmadizadeh M, Mosqueda G, Reinhorn A (2008): Compensation of actuator lag and dynamics for real-time hybrid structural simulation, Earthquake Engineering and Structural Dynamics, Vol.37, 21-42.

[5] Fujitani H, Sakae H, Kawasaki R, Fujii H, Hiwatashi T, Saito T (2008): Verification of real-time hybrid tests of response control of base isolation system by MR damper comparing shaking table tests, Proceedings of the SPIE's 15th Annual International Symposium on Smart Structures and Materials, No. 6932-161.

[6] Fujitani H, Sakae H, Ito M, Kawasaki R, Masutani A, Fujii H, Hiwatashi T (2008): The capability of the MR damper verified by shaking table tests and real time hybrid tests, Proceedings of the 14th World Conference on Earthquake Engineering, No.11-0088.

[7] Ito A, Kawasaki R, Fujitani H (2011): Effectiveness of real time hybrid test in semi-active controlled base isolation system, Journal of Structural and Construction Engineering (Transaction of Architectural Institute of Japan), 76 (663), 891-897. (in Japanese)

[8] Asai T, Chang CM, Spencer Jr. BF (2015): Real-Time Hybrid Simulation of a Smart Base-Isolated Building, Journal of Engineering Mechanics, ASCE, Vol.141, No.3.

[9] Tomizawa T, Fujitani H, Ito M, Aoyama Y, Shibata K, Sato Y (2014): Response Control by Using Rotary Inertia Mass Damper Filled with Magnetorheological Fluid, Journal of Structural and Construction Engineering (Transaction of Architectural Institute of Japan), 79 (704), 1435-1444. (in Japanese)

[10] Tomizawa T, Takahashi O, Fujitani H, Shibata K, Sato Y (2013): Performance tests of Rotary inertia Mass damper using magnetorheological fluid and its analytical verification, Journal of Structural and Construction Engineering (Transaction of Architectural Institute of Japan), 78(693), 1859-1867. (in Japanese)